1994ApJS...92..163S

THE ASTROPHYSICAL JOURNAL SUPPLEMENT SERIES, 92:163–172, 1994 May
© 1994. The American Astronomical Society. All rights reserved. Printed in U.S.A.

# A CATALOG OF BRIGHT-RIMMED CLOUDS WITH *IRAS* POINT SOURCES: CANDIDATES FOR STAR FORMATION BY RADIATION-DRIVEN IMPLOSION. II. THE SOUTHERN HEMISPHERE

KOJI SUGITANI
College of General Education, Nagoya City University, Mizuho-ku, Nagoya 467, Japan
AND
KATSUO OGURA
Kokugakuin University, Higashi, Shibuya-ku, Tokyo 150, Japan
*Received 1993 July 28; accepted 1993 September 30*

## ABSTRACT

Forty-five bright-rimmed clouds associated with *IRAS* point sources have been selected in the southern hemisphere from the ESO (R) Atlas in addition to the 44 objects of the northern work (Paper I). Again they are good candidates for the sites of star formation induced by radiation-driven implosion. Four of them are known to be associated with HH objects, and three with molecular outflows. Most of their sizes are $\lesssim 1$ pc, and the luminosities of the associated *IRAS* sources, $\sim 20$ to $3 \times 10^4\ L_\odot$, are much larger than those of the *IRAS* sources associated with Bok globules or dense cores in dark cloud complexes, both having a similar mass range. This suggests that intermediate-mass stars or multiple-star systems are mainly formed in bright-rimmed clouds. *IRAS* luminosity to cloud mass ratios are significantly greater than those in Bok globules or dense cores. The results confirm most of the findings of Paper I.

*Subject headings:* catalogs — H II regions — stars: formation — infrared: stars

## 1. INTRODUCTION

In the northern hemisphere, we surveyed the Palomar Observatory Sky Survey (POSS) prints for small bright-rimmed clouds (i.e., cometary globules or small molecular clouds surrounded by bright rims) associated with *IRAS* point sources (Sugitani, Fukui, & Ogura 1991; hereafter Paper I). As a result, we cataloged 44 such clouds and suggested that the bright-rimmed clouds with *IRAS* point sources are good candidates for star formation induced by radiation-driven implosion. This and related phenomena have recently been reviewed by Elmegreen (1993).

Since the publication of Paper I, some observations on star formation in bright-rimmed clouds have been reported. In the radio wavelengths, Patel, Xie, & Goldsmith (1994) mapped molecular clouds around cloud No. 24 of Paper I in the Rosette nebula. Tauber, Lis, & Goldsmith (1992) made a detailed study of bright-rimmed clumps in NGC 2264. They suggested that the physical conditions well match the predictions of the radiation-driven implosion model of Bertoldi (1989), and Bertoldi & McKee (1991). Cernicharo et al. (1992) made radio and optical observations of Ori I-2 (cloud No. 20) that was previously studied by Sugitani et al. (1989). Chernin & Masson (1991), and Olberg, Reipurth, & Booth (1992) revealed the presence of a molecular outflow in the bright-rimmed cometary globule ESO 210-6A associated with HH 46/47. Near-IR array cameras were used to map the Paper I clouds Nos. 5 and 44 (Skrutskie et al. 1991; Ressler & Shure 1991), and it is reported that small clusters or multiple-star systems have been formed in the small regions around the *IRAS* positions. In the southern sky, similar examples include the bright-rimmed clouds CG 30 (having HH 120) and ESO 210-6A (Graham & Heyer 1989). All these bright-rimmed clouds are associated with *IRAS* point sources and are considered to offer good evidence of star formation induced by radiation-driven implosion.

As Patel, Xie, & Goldsmith (1994) pointed out, some of the important physical parameters of molecular clouds, e.g., mass, kinematics, and density, cannot be derived by optical-based surveys like Paper I and this work. However, such surveys have an advantage of being done quickly, easily, and extensively, even if they can miss some bright-rimmed clouds due to contamination and/or extinction in optical wavelengths. Also they serve as guides for further observations in other wavelengths.

We have surveyed the southern hemisphere for bright-rimmed clouds associated with *IRAS* point sources in continuation to Paper I in order to improve the statistics. The results are presented here as an additional catalog of such clouds together with some discussion on star formation in this sort of clouds. We also present, in Appendix, the results of an outflow survey of the clouds cataloged in Paper I, which was carried out with the KOSMA 3 m telescope in order to indicate that bright-rimmed clouds with *IRAS* point sources are really sites of star formation.

## 2. SAMPLING STRATEGY

In the southern hemisphere ($\delta \lesssim -20°$) we have examined all the published ESO(R) Atlas in search of bright-rimmed clouds, whereas in the northern hemisphere the inspection was made mainly around H II regions with sizes of $\geq 60'$. We have used the SERC(J) Atlas in a few areas where the ESO(R) Atlas has not yet been published. Since the ESO(R) and SERC(J) Atlases are in the form of film copy, their photographic quality is much better than that of the POSS prints used in the north-



© American Astronomical Society • Provided by the NASA Astrophysics Data System

1994ApJS...92..163S



ern sky. This considerably improved the detectability of small/faint bright-rimmed clouds.

The *IRAS* Point Source Catalog (Joint *IRAS* Science Working Group 1988) was used to select the bright-rimmed clouds associated with infrared sources. Only those clouds which have *IRAS* sources *surrounded* by curved bright rims have been included, and the clouds which have *IRAS* sources located just on the bright rims have been rejected in order to exclude the sources which are not of stellar origin but emission from dust condensations.

Note that not all the clouds surrounded by a curved rim (ionization front) and having an *IRAS* source are sampled depending on their viewing geometry. If a rim is more or less concentric of an *IRAS* source, the source will always appears near the center of the rim. But the bright rim will show up or disappear depending on the viewing angle; if it is viewed nearly from the front or the back on its axis of symmetry, it may not show up as a bright rim on sky atlases. It is, however, not easy to estimate accurately what fraction of the whole solid angle ($4\pi$) the adequate viewing angle can be, owing to the variety of the rim shape, but we roughly guess it is $\sim\frac{2}{3}$. In other words, there will exist a factor of $\sim$1.5 more bright-rimmed clouds that meet our criteria than those we actually picked up in the same volume in our Galaxy.

Some additional criteria were laid on the qualities of the *IRAS* fluxes to exclude emission from diffuse dust. As in Paper I we have included only sources that are detected at least at two *IRAS* bands and that have point source correlation coefficients (CC) of F or better at 25 $\mu$m, where the CC is an index of the degree for the source to be a point source and *IRAS* point sources have CC between 87% and 100% which are encoded as A = 100%, B = 99%, N = 87% (see the Explanatory Supplement of the *IRAS* Catalog; Beichman et al. 1988). No criteria for confusion and cirrus flag were imposed. Contrary to Paper I, however, the criterion of detection at 25 $\mu$m was not applied here. Due to these criteria of the *IRAS* detections which are slightly generous compared to those in Paper I, seven sources have been included which would have otherwise been excluded.

## 3. RESULTS

We have selected 45 bright-rimmed clouds associated with *IRAS* point sources in/around altogether 22 H II regions. Table 1 presents the H II regions where the bright-rimmed clouds associated with *IRAS* point sources are selected. The catalog of the bright-rimmed clouds is given in Table 2. The identification numbers are given in continuation to the last one used in Paper I. The properties of the *IRAS* sources are listed in Table 3 together with additional information on associated Herbig-Haro (HH) objects and molecular outflows. The finding charts reproduced from the ESO (R) Atlas are shown in Figure 1 (Plates 1–7). The location of the *IRAS* point source is indicated by a pair of white or black tips. The accuracy of the location should be better than 10″, which is slightly better than that in Paper I. This is mainly due to the fact that here we used the Guide Star Catalog (Space Telescope Science Institute 1989), which has a larger number of positional standard stars than the SAO Catalog used in Paper I.

TABLE 1

H II REGIONS WHERE BRIGHT-RIMMED CLOUDS WITH IRAS POINT SOURCES WERE SELECTED

| H II Region | Size (arcmin.) | $d$ (kpc) | Ref. of $d$ | Related Object |
|---|---|---|---|---|
| S306 | 30 | 4.40 | 1 | |
| S307 | 6 | 2.45 | 1 | |
| RCW14 | 60×20 | 1.55 | 1 | S310? |
| Gum Nebula | 2000×2000 | 0.45 | 2 | |
| NGC2626 | 100×110 | 0.95 | 3 | Pup R2 |
| RCW27 | 100×100 | 1.15 | 1 | |
| RCW32 | 27×27 | 0.70 | 1 | |
| RCW38 | 40×40 | 1.20 | 4 | vdB26 |
| NGC3503 | 120×80 | 2.88 | 5 | Car R1 |
| BBW347 | 45×45 | 2.70 | 6 | Stock 13 |
| RCW62 | 80×80 | 1.66 | 7 | IC2944 |
| (Cen R1) | 30×70 | 2.00 | 3 | vdB 59 |
| RCW75 | 18×13 | 1.90 | 8 | Stock 16 |
| RCW85 | 25×20 | 1.17 | 1 | |
| RCW98 | 6×5 | 3.60 | 1 | |
| RCW105 | 45×35 | 1.80 | 1 | |
| ($\sigma$ Sco) | 50×30 | 1.65 | 9 | $\rho$-Oph, S9 |
| RCW108 | 210×120 | 1.32 | 10 | NGC6193, Ara OB1, Ara R1 |
| RCW113/116 | 360×300 | 1.75 | 11 | NGC6231, Sco OB1, Sco R4 |
| RCW134 | 60×50 | 1.26 | 3 | Sco R7 |
| M8 | 90×60 | 1.38 | 12 | NGC6530 |
| Simeis 188 | 40×45 | 1.38 | 13 | |

REFERENCES.—(1) Georgelin, Georgelin, & Roux 1973; (2) Graham 1986; (3) Herbst 1975a; (4) Georgelin & Georgelin 1976; (5) Herbst 1975b; (6) Ogura & Walsh 1992; (7) Ardeberg & Maurice 1980; (8) Turner 1985; (9) Chini 1981; (10) Herbst & Havlen 1977; (11) Seggewiss 1968; (12) Kilambi 1977; (13) Herbst et al. 1982.

### 3.1. *Bright-rimmed Clouds*

Following Paper I, the bright-rimmed clouds are classified into three types according to their rim morphology (1) type A: moderately curved rim, (2) type B: tightly curved rim, and (3) type C: cometary rim. Their rim sizes, length ($l$) and width ($w$), are defined as in Figure 2 of Paper I. Type A should have a length to width ratio, $l/w$, less than 0.5, and type B greater than 0.5. Generally a bright-rimmed cloud appears to be composed of a dense head/core part and a less dense tail. Star formation should occur in the dense head part. We made a rough estimate of the radii of the heads based on the sizes measured above. Assuming a round shape of the head, its "radius" $R$ has been defined as follows: (1) type A: $R = l/2$, (2) type B: $R = w/4$, and (3) type C: $R = w/2$. All the radii estimated are $\lesssim$1.2 pc and 78% of them are $\lesssim$0.5 pc, as shown in Figure 2. Following § 3.1 of Paper I, we have estimated the masses contained in the head parts of the clouds $M'_{\rm cloud}$ by $M'_{\rm cloud} = \frac{4}{3}\pi R^3\, mn$, where $R$ is the radius defined above, $m$ the hydrogen molecular weight, and $n$ the assumed number density of $3 \times 10^4$ $H_2$/cc, which is the average density derived from the $^{13}$CO observations of the three bright-rimmed clouds, Ori I-2, IC1396 rim E, and L1206 (Sugitani et al. 1989). The range of the $M'_{\rm cloud}$ is $\sim 0.1$–$10^4$ $M_\odot$, with $\sim$40% of them less than 100 $M_\odot$ and $\sim$60% less than 350 $M_\odot$. Table 4 summarizes the average lengths, widths, radii, and cloud masses as well as the range of the radii as a function of rim type. Both the average radii and the logarithmic averages of the cloud masses are larger than those in Paper I, which are $0.18 \pm 0.10$ pc and $1.2 \pm 0.7$ for type A, $0.31 \pm 0.21$ pc and $1.7 \pm 1.0$ for type B, and $0.09 \pm 0.01$ pc and $0.31 \pm 0.14$ for type C, respectively.

© American Astronomical Society • Provided by the NASA Astrophysics Data System

1994ApJS...92..163S



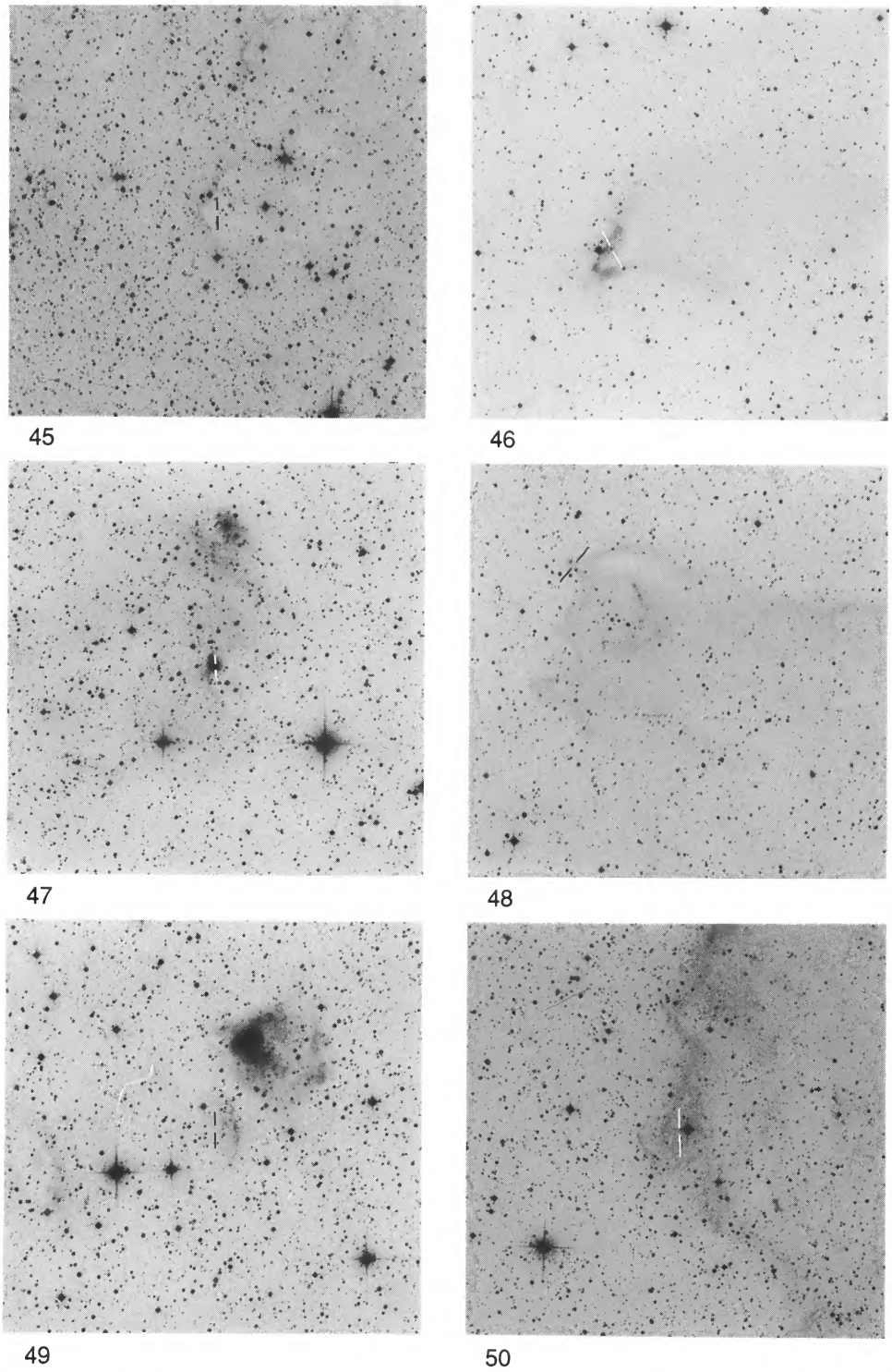


FIG. 1.—Finding charts for the bright-rimmed clouds in the southern sky. The charts are reproduced from the ESO(R) Atlas. The position of the *IRAS* point source associated with the bright-rimmed cloud is indicated by a pair of white or black tips. 1 mm in the charts corresponds to 0:28.

See SUGITANI & OGURA (92, 164)

© American Astronomical Society • Provided by the NASA Astrophysics Data System

1994ApJS...92..163S

PLATE 2

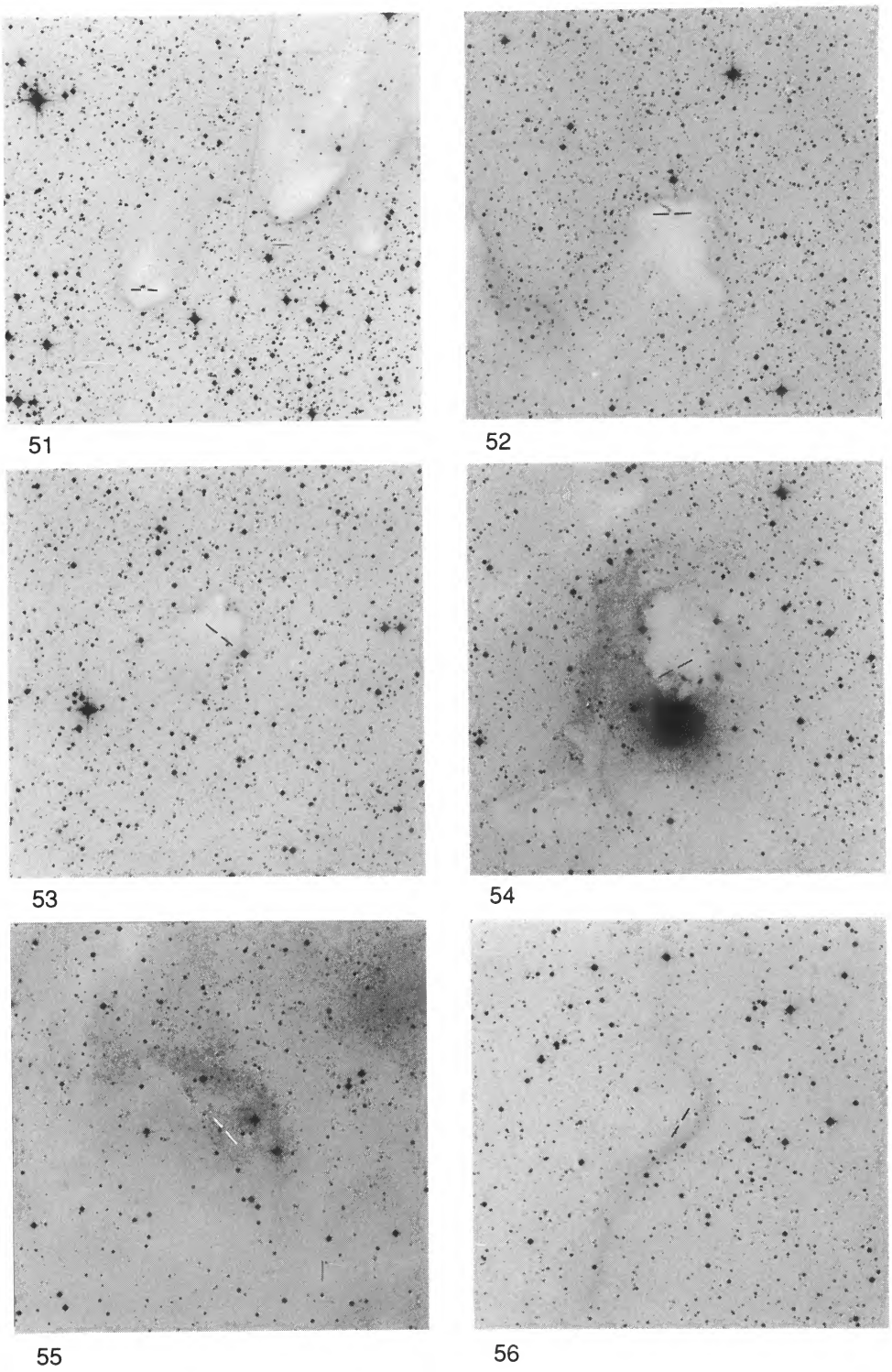


FIG. 1—*Continued*

See SUGITANI & OGURA (92, 164)

© American Astronomical Society • Provided by the NASA Astrophysics Data System

1994ApJS...92..163S



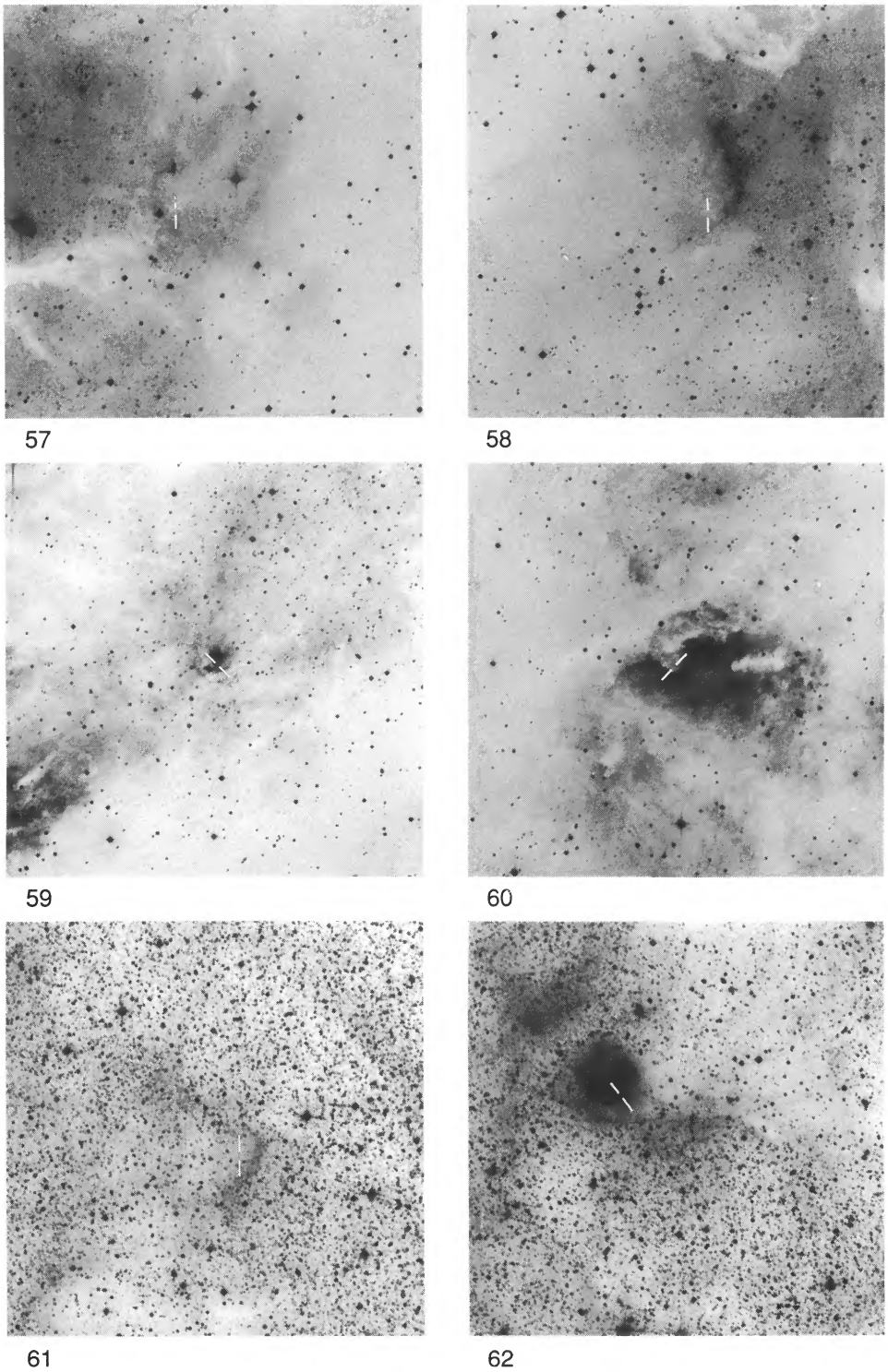


FIG. 1—*Continued*

See SUGITANI & OGURA (92, 164)

© American Astronomical Society • Provided by the NASA Astrophysics Data System

1994ApJS...92..163S

PLATE 4

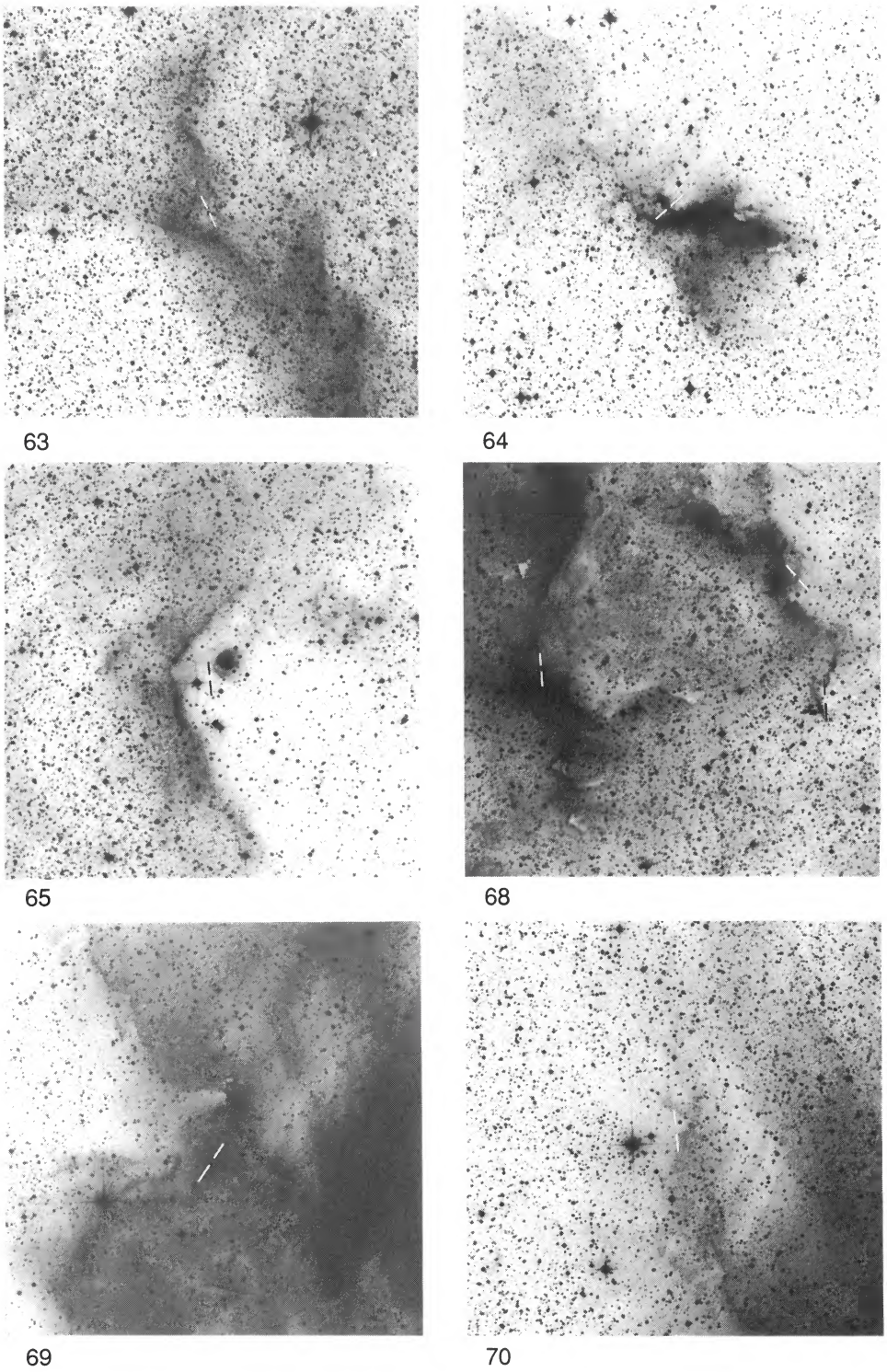


FIG. 1—*Continued*

See SUGITANI & OGURA (92, 164)

© American Astronomical Society • Provided by the NASA Astrophysics Data System

1994ApJS...92..163S



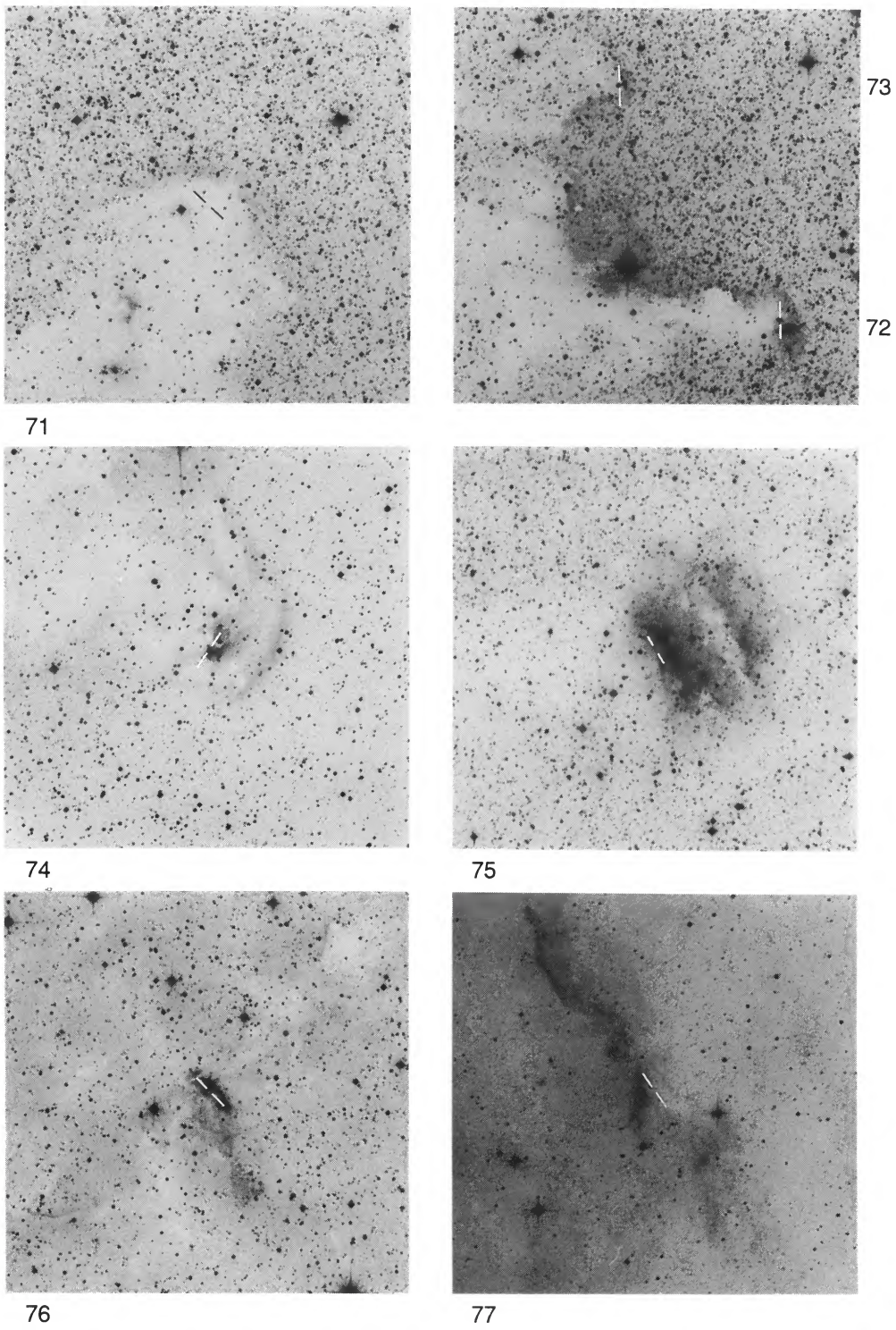


FIG. 1—*Continued*

See SUGITANI & OGURA (92, 164)

© American Astronomical Society • Provided by the NASA Astrophysics Data System

1994ApJS...92..163S

PLATE 6

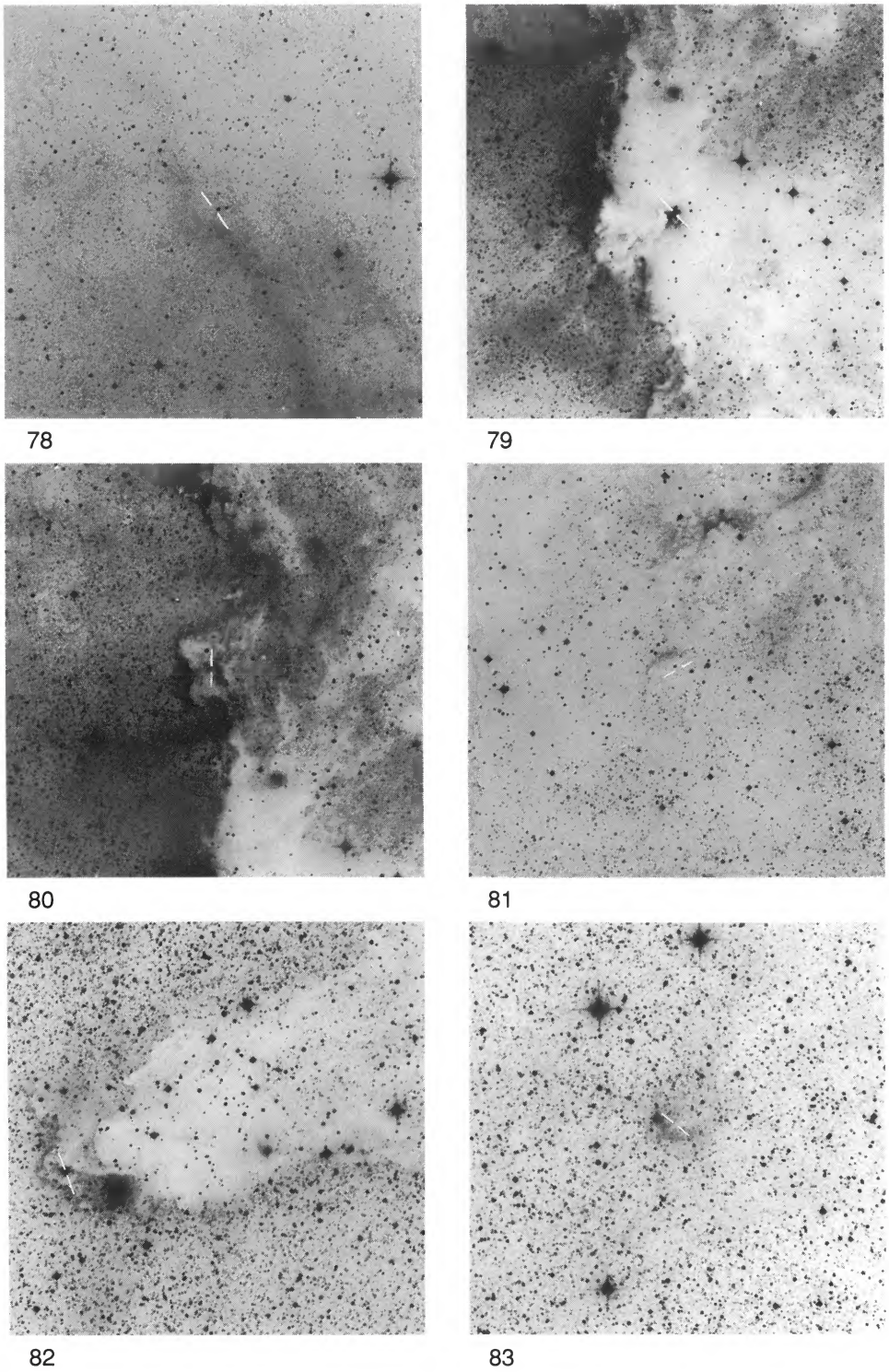


FIG. 1—*Continued*

See SUGITANI & OGURA (92, 164)

© American Astronomical Society • Provided by the NASA Astrophysics Data System

1994ApJS...92..163S



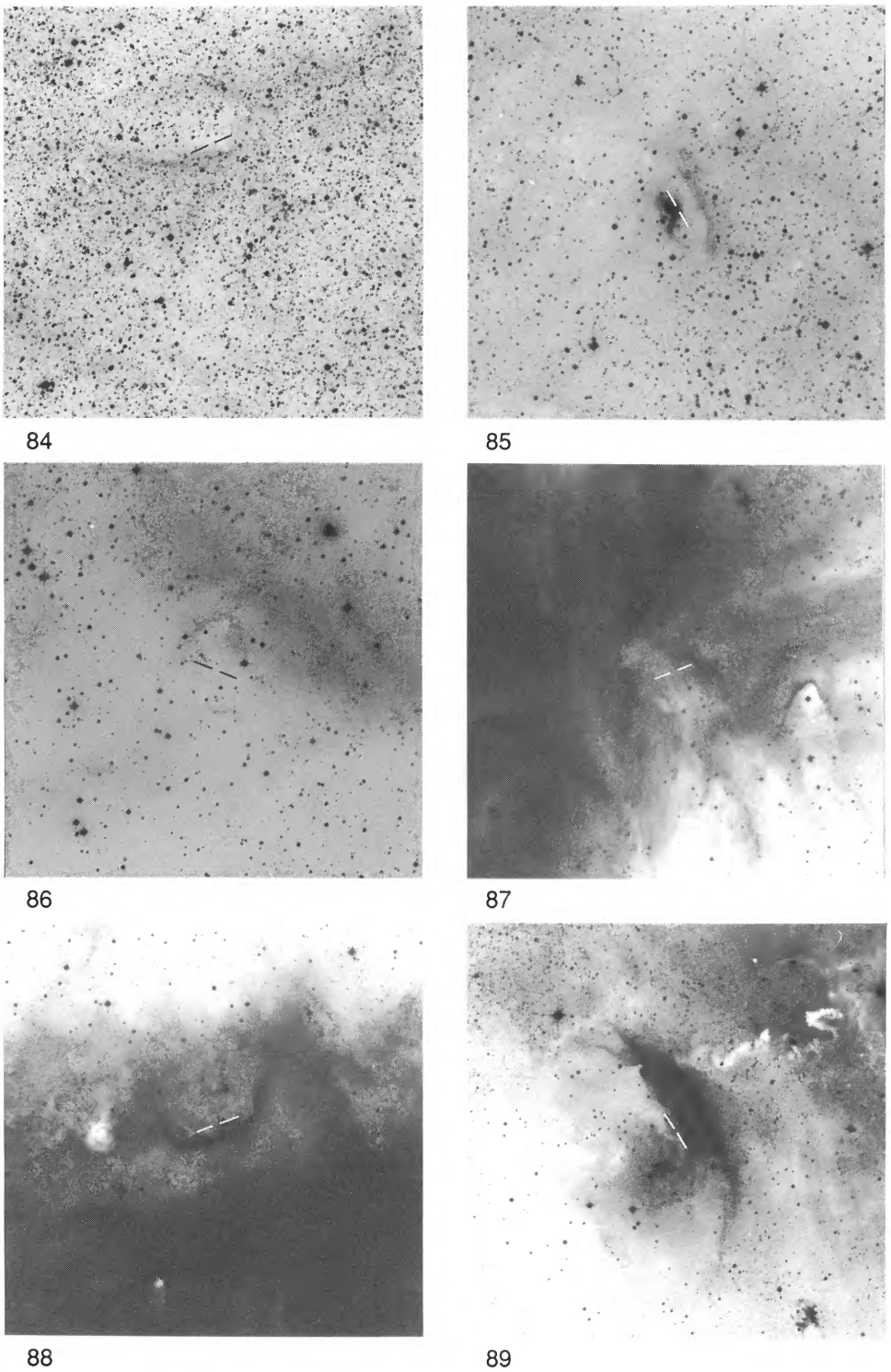


FIG. 1—*Continued*

See SUGITANI & OGURA (92, 164)

© American Astronomical Society • Provided by the NASA Astrophysics Data System

1994ApJS...92..163S



TABLE 2

BRIGHT-RIMMED CLOUDS ASSOCIATED WITH *IRAS* POINT SOURCES

| Cloud Number (1) | HII Region (2) | Rim Type (3) | $l$ (pc) (4) | $w$ (pc) (5) | α (1950) (6) | δ (1950) (7) | *IRAS* Source (8) | Other Name (9) |
|---|---|---|---|---|---|---|---|---|
| 45 | RCW14 | A | 0.60 | 1.74 | 7h16m15.5s | -22°00'41" | 07162-2200 | |
| 46 | Gum Neb. | B | 0.20 | 0.20 | 7h17m54.0s | -44°29'24" | 07178-4429 | CG1 |
| 47 | S306 | A | 0.72 | 2.90 | 7h29m36.9s | -19°21'07" | 07296-1921 | |
| 48 | Gum Neb. | B | 0.20 | 0.38 | 7h32m56.6s | -46°47'34" | 07329-4647 | CG4 |
| 49 | S307 | A | 0.60 | 2.49 | 7h33m28.0s | -18°42'17" | 07334-1842 | |
| 50 | Gum Neb. | B | 0.24 | 0.20 | 7h38m51.4s | -42°59'18" | 07388-4259 | |
| 51 | Gum Neb. | C | 0.68 | 0.31 | 8h07m40.2s | -35°56'07" | 08076-3556 | CG30 |
| 52 | Gum Neb. | C | 0.55 | 0.40 | 8h24m16.5s | -50°50'44" | 08242-5050 | GDC1 |
| 53 | Gum Neb. | B | 0.27 | 0.35 | 8h25m03.4s | -50°30'34" | 08250-5030 | GDC4 |
| 54 | NGC2626 | A | 0.42 | 1.26 | 8h33m42.6s | -40°28'02" | 08337-4028 | |
| 55 | RCW27 | A | 0.96 | 2.90 | 8h39m23.4s | -40°41'18" | 08393-4041 | |
| 56 | RCW27 | A | 0.70 | 1.64 | 8h41m08.3s | -39°49'05" | 08411-3949 | |
| 57 | RCW32 | A | 0.20 | 0.66 | 8h42m18.2s | -41°05'19" | 08423-4105 | |
| 58 | RCW32 | A | 0.35 | 0.93 | 8h43m35.7s | -41°05'03" | 08435-4105 | |
| 59 | RCW38 | A | 0.16 | 0.37 | 8h56m22.3s | -47°11'17" | 08563-4711 | |
| 60 | RCW38 | B | 0.33 | 0.47 | 8h58m19.1s | -47°19'51" | 08583-4719 | |
| 61 | NGC3503 | B | 1.73 | 3.25 | 10h58m09.5s | -59°20'02" | 10581-5920 | |
| 62 | NGC3503 | B | 4.30 | 4.13 | 10h59m11.6s | -59°34'52" | 10591-5934 | |
| 63 | NGC3503 | A | 1.14 | 3.01 | 11h01m13.5s | -59°31'50" | 11012-5931 | |
| 64 | BBW347 | A | 1.49 | 3.69 | 11h10m07.4s | -58°29'60" | 11101-5829 | |
| 65 | RCW62 | A | 1.48 | 4.80 | 11h30m37.9s | -63°11'24" | 11306-6311 | |
| 66 | RCW62 | A | 0.32 | 0.73 | 11h31m31.4s | -62°59'45" | 11315-6259 | |
| 67 | RCW62 | A | 0.70 | 2.05 | 11h31m42.5s | -62°54'43" | 11317-6254 | |
| 68 | RCW62 | A | 0.76 | 2.54 | 11h33m12.9s | -62°58'15" | 11332-6258 | |
| 69 | RCW62 | B | 1.96 | 2.70 | 11h38m49.0s | -63°06'34" | 11388-6306 | |
| 70 | RCW62 | B | 0.58 | 1.24 | 11h39m48.3s | -62°51'11" | 11398-6251 | |
| 71 | (Cen R1) | A | 1.22 | 3.74 | 13h05m02.8s | -61°54'26" | 13050-6154 | |
| 72 | RCW75 | C | ... | 1.08 | 13h15m51.5s | -62°17'58" | 13158-6217 | |
| 73 | RCW75 | A | 0.54 | 1.39 | 13h16m49.3s | -62°08'19" | 13168-6208 | |
| 74 | RCW85 | A | 0.98 | 2.38 | 14h15m59.2s | -61°11'30" | 14159-6111 | |
| 75 | RCW98 | A | 0.44 | 2.55 | 15h51m56.5s | -54°30'14" | 15519-5430 | |
| 76 | RCW105 | A | 0.23 | 1.20 | 16h06m56.7s | -48°58'04" | 16069-4858 | |
| 77 | (σ Sco) | A | 0.04 | 0.17 | 16h16m51.3s | -25°26'29" | 16168-2526 | |
| 78 | (σ Sco) | A | 0.05 | 0.13 | 16h17m50.8s | -25°01'01" | 16178-2501 | |
| 79 | RCW108 | A | 1.32 | 5.04 | 16h36m14.8s | -48°45'54" | 16362-4845 | |
| 80 | RCW108 | A | 0.56 | 1.13 | 16h36m31.8s | -48°36'35" | 16365-4836 | |
| 81 | RCW108 | A | 0.38 | 1.06 | 16h37m22.2s | -49°11'59" | 16373-4911 | |
| 82 | RCW113/116 | B | 0.88 | 0.95 | 16h43m21.0s | -41°08'32" | 16438-4110 | |
| 83 | RCW113/116 | A | 0.38 | 0.94 | 16h48m43.2s | -40°43'09" | 16487-4043 | |
| 84 | RCW113/116 | A | 0.80 | 2.77 | 16h50m17.5s | -40°02'29" | 16502-4002 | |
| 85 | RCW113/116 | A | 0.54 | 2.59 | 16h55m33.3s | -42°37'33" | 16555-4237 | |
| 86 | RCW134 | B | 0.86 | 1.43 | 17h46m21.5s | -31°28'20" | 17463-3128 | |
| 87 | M8 | B | 1.35 | 1.71 | 17h59m47.5s | -24°22'14" | 17597-2422 | |
| 88 | M8 | A | 0.81 | 1.85 | 18h01m13.1s | -24°07'11" | 18012-2407 | |
| 89 | Simeis 188 | A | 0.19 | 0.92 | 18h06m50.7s | -24°05'33" | 18068-2405 | |

NOTES.—Col. (2): H II region where the bright-rimmed cloud is selected. Col. (3): Morphological type of the bright rim (see § 3.1). Cols. (4)–(5): Length and width of the bright rim. Cols. (6)–(7): 1950 coordinates which are quoted from the positions in the *IRAS* Point Source Catalog. Col. (8): *IRAS* point source associated with the bright-rimmed cloud.

### 3.2. *Associated IRAS Point Sources*

Figure 3 shows the 12/25/60 μm color-color diagram for the 31 *IRAS* sources, excluding 14 sources not detected at 25 and/or 60 μm. As in Paper I, the *IRAS* sources are classified into two types on this diagram. One type includes those sources with a color distribution similar to that of core samples, which are considered to be newly formed or still-forming stars embedded in their parental clouds (Beichman 1983). The other type comprises samples with a color distribution similar to that of hot cirrus sources, which are considered to be compact structures of cirri. Following Paper I, we refer to the former as type I and to the latter as type II. The numbers of type I and type II sources are 17 and 14, respectively. With an average value of 99.9%, the point source correlation coefficients at 25 μm of the type I sources are very high (see the col. [7] of Table 3). The coefficients of the type II sources are still rather high, with an average value of 97.7% at 25 μm. The 14 sources that are not detected at 25 and/or 60 μm (four of them are not detected at 100 μm as well) have again high correlation coefficients, the average being 98.4% at 25 μm. We refer to these 14 sources as type III.

We have derived the luminosities $L_{IR}$ of the *IRAS* sources (Table 3), following Myers et al. (1987). In order to examine

© American Astronomical Society • Provided by the NASA Astrophysics Data System

1994ApJS...92..163S



TABLE 3

PROPERTIES OF *IRAS* POINT SOURCES

| Number (1) | *IRAS* Source (2) | 12 μm (3) | 25 μm (4) | 60 μm (5) | 100 μm (6) | CC (7) | Type (8) | $L_{IR}$ ($L_\odot$) (9) | HH/Outflow (10) | Ref. (11) |
|---|---|---|---|---|---|---|---|---|---|---|
| 45 | 07162-2200 | 0.25 L | 0.31 L | 2.08: | 10.59 | ...CEB | III | (30) | | |
| 46 | 07178-4429 | 6.68 | 7.60 | 13.12 | 33.59 | AAAA | I | 20 | | |
| 47 | 07296-1921 | 4.73 | 16.19 | 53.10 | 330.90 L | AAAD | I | (8400) | | |
| 48 | 07329-4647 | 0.25 L | 0.38 | 1.34 | 5.82 L | FBA... | I | (0.83) | | |
| 49 | 07334-1842 | 5.98 | 53.90 | 234.73 | 452.08 L | AAAB | I | (4300) | | |
| 50 | 07388-4259 | 0.25 L | 0.25 L | 1.72: | 9.59 | JFEA | III | (2.2) | | |
| 51 | 08076-3556 | 0.63 | 3.73 | 18.25 | 47.54: | BAAA | I | 16 | HH120 | 1 |
| 52 | 08242-5050 | 0.82 | 6.31 | 26.13 | 58.27: | BAAA | I | 22 | HH46/47 | 2, 3, 4 |
| 53 | 08250-5030 | 0.25 L | 0.25 L | 1.20 | 17.08 | ...BA... | III | (3.4) | | |
| 54 | 08337-4028 | 0.25 L | 39.95 | 347.61 L | 1266.04: | LAAF | III | (1100) | HH132 | 5, 6 |
| 55 | 08393-4041 | 1.30 | 4.90 | 65.17 | 171.53 | EAAB | I | 350 | | |
| 56 | 08411-3949 | 0.37 L | 0.26 | 3.45: | 13.16 | BDBB | II | 23 | | |
| 57 | 08423-4105 | 2.92: | 3.80: | 98.13 L | 452.21 | CAGC | III | (210) | | |
| 58 | 08435-4105 | 2.89 | 3.80: | 49.70: | 224.89: | DEFD | II | 140 | | |
| 59 | 08563-4711 | 51.90 | 441.82 | 3298.50 | 3153.86 | DBAA | I | 13000 | | |
| 60 | 08583-4719 | 6.77 | 34.08: | 468.83 L | 1691.72 L | BBCE | III | (280) | | |
| 61 | 10581-5920 | 1.20 | 1.51 | 11.04: | 87.98: | CBBA | II | 750 | | |
| 62 | 10591-5934 | 19.98: | 41.82 | 743.41 | 1313.66 | DDCA | II | 18000 | | |
| 63 | 11012-5931 | 0.56 L | 0.81 L | 8.63: | 26.97 | GECC | III | (170) | | |
| 64 | 11101-5829 | 9.00 | 130.35 | 618.19 | 750.21 | BAAA | I | 14000 | HH135/136 | 7 |
| 65 | 11306-6311 | 2.31: | 12.74 | 104.84 | 231.62: | BBCA | I | 1100 | | |
| 66 | 11315-6259 | 0.84 | 1.54 | 25.63 | 239.38 L | BBAC | II | (190) | | |
| 67 | 11317-6254 | 2.83: | 4.69 | 62.97: | 239.38 L | DDBA | II | (470) | | |
| 68 | 11332-6258 | 6.93 | 37.40 | 479.08 | 1162.64 L | BAAA | I | (3400) | | |
| 69 | 11388-6306 | 5.33 L | 9.26 | 171.17 L | 504.31: | CBFD | III | (1300) | | |
| 70 | 11398-6251 | 1.44: | 1.40 | 30.70: | 138.33 | DCDA | II | 490 | | |
| 71 | 13050-6154 | 1.43 L | 11.06 | 82.84 | 256.72 | HAAA | I | 1500 | | |
| 72 | 13158-6217 | 8.99 | 22.45 | 167.51 | 443.78 L | BADB | I | (1800) | | |
| 73 | 13168-6208 | 1.18 | 3.47 | 18.62 | 90.54 L | BABF | I | (210) | | |
| 74 | 14159-6111 | 9.85 L | 44.99: | 1143.87: | 2562.89 | EDEB | II | 5500 | | |
| 75 | 15519-5430 | 10.71 | 23.93: | 614.81 | 1816.49 | BDBB | II | 34000 | | |
| 76 | 16069-4858 | 14.99 | 55.79 | 472.94 | 938.09: | AABB | I | 5600 | | |
| 77 | 16168-2526 | 0.75 | 1.44: | 49.42: | 112.15 L | DFDA | II | (3.1) | | |
| 78 | 16178-2501 | 0.39 | 0.74: | 20.90 L | 65.47 L | FBFD | III | (0.14) | | |
| 79 | 16362-4845 | 208.29 | 2977.72 | 12219.98 L | 18723.71 | BAAA | III | (4400) | | |
| 80 | 16365-4836 | 1.62 | 2.29: | 48.48: | 138.18 L | ACEE | II | (220) | | |
| 81 | 16373-4911 | 1.08 L | 2.96 L | 9.42 | 131.76 L | DAA... | III | (38) | | |
| 82 | 16438-4110 | 7.41 | 9.57 | 178.50: | 1004.79 L | AADC | II | (1500) | | |
| 83 | 16487-4043 | 0.94 | 1.16 | 11.81 | 29.05 L | CBB... | II | (110) | | |
| 84 | 16502-4002 | 3.18 | 3.44 | 20.76 | 106.75 | CBBB | II | 450 | | |
| 85 | 16555-4237 | 94.91 | 251.87 | 1917.72 | 2212.96 | AAAB | I | 18000 | | |
| 86 | 17463-3128 | 3.12 L | 23.39 | 166.70 | 289.78 | CAAA | I | 880 | | |
| 87 | 17597-2422 | 3.36 | 4.42 | 109.65 L | 811.98: | DCAF | III | (1400) | | |
| 88 | 18012-2407 | 49.56 L | 64.55 L | 513.54 L | 1307.14 | DDCA | III | (2200) | | |
| 89 | 18068-2405 | 2.19 | 1.98 L | 224.05 L | 629.41 L | BC..... | III | (39) | | |

NOTES.—Col. (1): identification number. Col. (2): name of the *IRAS* point source. Cols. (3)–(6): *IRAS* fluxes at the four wavelengths, where "L" and ":" denote upper limit and moderate quality, respectively. Col. (7): correlation coefficients of the *IRAS* point source. Col. (8): classification of the *IRAS* point source according to its colors (see § 3.2). Col. (9): luminosity of the *IRAS* point source, where the parentheses denote the *IRAS* source with upper limit fluxes at 60 μm and/or 100 μm. Cols. (10)–(11): known molecular outflow or HH object associated with the *IRAS* point source and its reference.

REFERENCES.—(1) Petterson 1984; (2) Schwartz 1977; (3) Chernin & Masson 1991; (4) Olberg, Reipurth, & Booth 1992; (5) Ogura 1990; (6) Iwata et al. 1993; (7) Ogura & Walsh 1992.

accurately the luminosity function of the *IRAS* sources, we use only the 19 *IRAS* sources whose fluxes are detected at least in the three bands centered at 25, 60, and 100 μm. The distribution of $L_{IR}$ for the 19 sources is shown in Figure 4, which indicates that it ranges from 16 to $3.4 \times 10^4\ L_\odot$. The logarithmic averages of the *IRAS* luminosities, $\log (L_{IR}/L_\odot)$, for the types A, B, and C clouds are $3.3 \pm 0.9$ (12), $2.8 \pm 1.0$ (5), and $1.3 \pm 0.1$ (2), respectively, where the numerals in the parentheses are the sample numbers. The average of the 19 sources is 3.0, which is one order of magnitude larger than that of Paper I and is more than two orders larger than that of the *IRAS* sources associated with Bok globules, 0.46 (Sugitani et al. 1989) or dense cores in molecular cloud complexes, 0.12 (Beichman et al. 1986).

## 4. DISCUSSIONS

### 4.1. *Comparisons with Paper I*

This survey covers one-third of the whole sky and has selected 45 sources. The criteria for selecting the sources in this survey slightly differ from those in Paper I. We have surveyed the whole sky area of $\delta \lesssim -20°$ in this survey, whereas mainly the regions in and around the H II regions with sizes of $\gtrsim 60'$ were surveyed in Paper I. This means that we might have biased toward nearby bright-rimmed clouds in the northern survey, whereas relatively distant clouds are also included in the southern survey. In addition, we have not applied the criterion of *IRAS* detection at 25 μm in this paper in contrast to Paper I. This could also bias the survey toward distant sources.

© American Astronomical Society • Provided by the NASA Astrophysics Data System

1994ApJS...92..163S



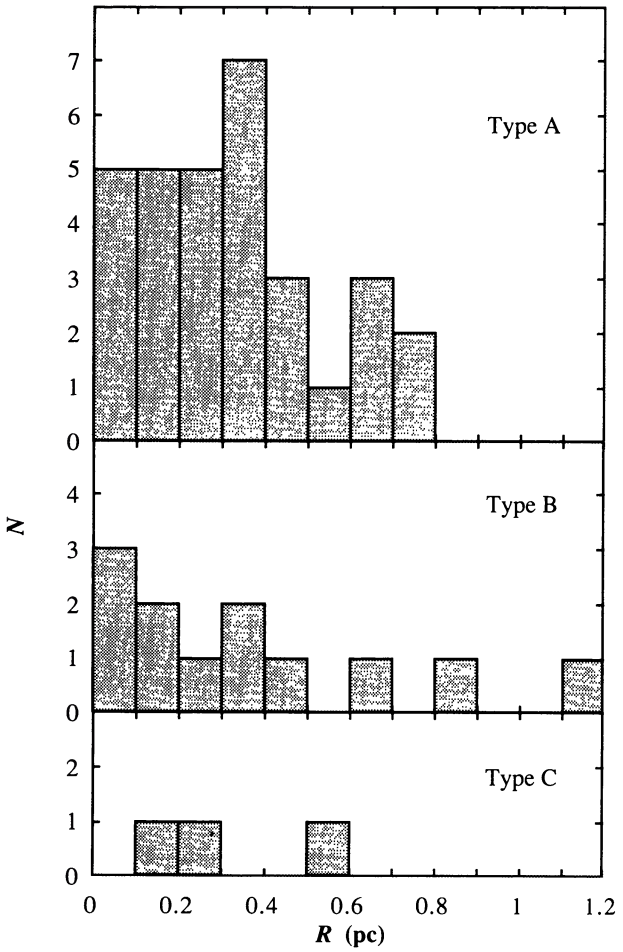


FIG. 2.—Distribution of the cloud radii estimated from the rim sizes (see text).

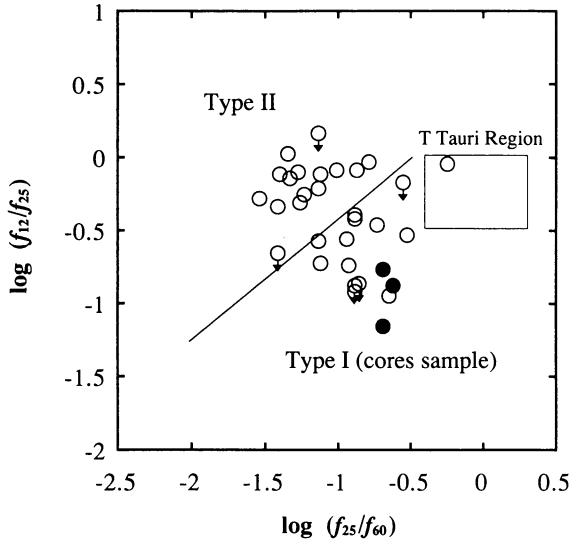


FIG. 3.—12/25/60 $\mu$m color-color diagram of the *IRAS* point sources. Filled circles denote the *IRAS* sources associated with HH objects and/or molecular outflows. Down arrows indicate upper limits at 12 $\mu$m. Type I sources have a distribution similar to that of the sources in the molecular cloud cores, and type II sources distribute similarly to hot cirri.

Thus, this slightly generous selection condition has provided nearly the same number of the sources in spite of the fact that only one-third of the whole sky is covered in this work. If we apply the same criteria in this survey, the total number of the detected clouds would be 25. This number is consistent with that expected from the result of the northern survey, $44 \times \frac{1}{2} = 22$, assuming a uniform distribution of the bright-rimmed clouds with *IRAS* point sources in the whole sky.

The average distance of all the 45 sources and that of the above 25 sources are 1.61 and 1.56 kpc, respectively. These values are larger than that of the 44 sources in the previous work, 1.16 kpc, indicating that this work reaches more distant sources. This difference may be due, in part, to the structure of the Galaxy; in the southern sky, two spiral arms of our Galaxy stretch away nearly along the line of sight. Also the large dynamic range of the ESO(R) Atlas has certainly contributed to the high detectability particularly of distant objects. The increase of distant clouds explains the larger average size and, therefore, the higher average mass of the selected clouds in this work, since we have picked up mainly objects with apparent sizes of a few arcminutes. Considering the detection limit of *IRAS,* the survey is thus likely to be biased toward the distant sources having high intrinsic luminosities.

### 4.2. *Properties of the IRAS Sources*

All the *IRAS* sources selected here are located toward the regions of high visual extinction on the ESO (R) Atlas and are considered to be good candidates for embedded young stellar objects on account of their high *IRAS* correlation coefficients. The type I sources are most likely young stellar objects embedded in molecular cloud cores as suggested in Paper I. However, as for signposts of recent star formation, only three of them, Nos. 51, 52, and 64, are known to be associated with HH

TABLE 4

PROPERTIES OF BRIGHT-RIMMED CLOUDS WITH *IRAS* POINT SOURCES

| Rim Type | Sample Number | $\bar{l}$ (pc) | $\bar{w}$ (pc) | $R$ Range (pc) | $\bar{R}$ (pc) | $\overline{\log (M/M_\odot)}$ |
|---|---|---|---|---|---|---|
| A ... | 30 | 0.64 ± 0.40 | 2.0 ± 1.3 | 0.02–0.74 | 0.32 ± 0.20 | 2.0 ± 1.1 |
| B ... | 12 | 1.1 ± 1.3 | 1.5 ± 1.3 | 0.05–1.10 | 0.37 ± 0.33 | 2.0 ± 1.3 |
| C ... | 3 | 0.61 ± 0.29[a] | 0.60 ± 0.34 | 0.15–0.54 | 0.30 ± 0.17 | 2.1 ± 0.7 |

[a] Except for the cloud No. 72, whose rim length ($l$) could not be determined.

© American Astronomical Society • Provided by the NASA Astrophysics Data System

1994ApJS...92..163S



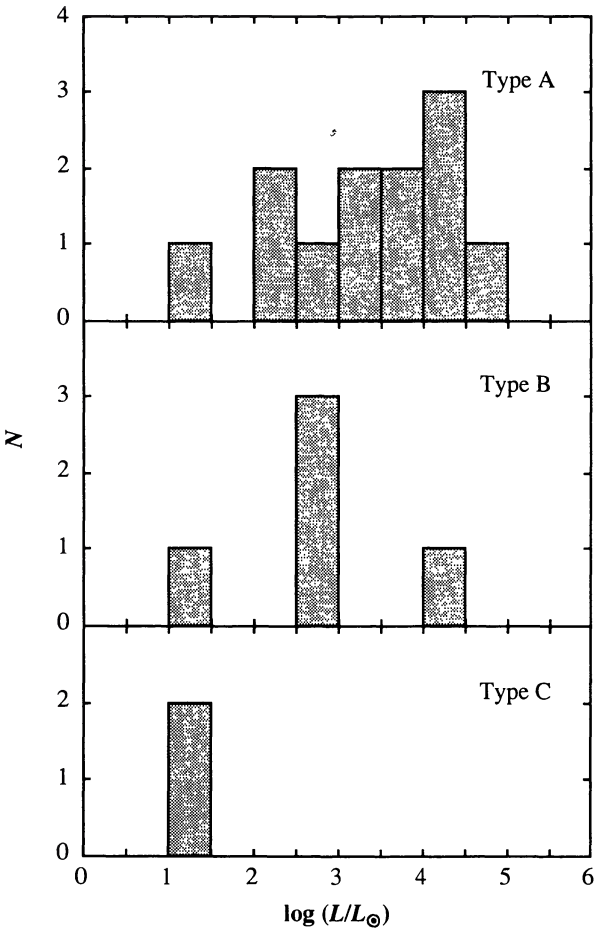


FIG. 4.—Distribution of the luminosities of the *IRAS* point sources.

objects or/and molecular outflows, HH120 (Pettersson 1984), HH46/47 (Reipurth & Heathcote 1991; Chernin & Masson 1991; Olberg, Reipurth, & Booth 1992), and HH135/136 (Ogura & Walsh 1992; Nakano et al. 1993), respectively.

On the *IRAS* color-color plots, the type II sources show a distribution of the *IRAS* color indices similar to that of the hot cirrus sources having warm 12/25 $\mu$m color indices. However, the fact that they lie in opaque regions and have high correlation coefficients suggests that they are also stellar objects. The bright-rimmed clouds are associated with H II regions and can, therefore, be strongly contaminated by extended infrared emission, particularly in the *IRAS* bands of longer wavelengths. This means that the 25/60 $\mu$m color indices could become spuriously smaller than their actual values due to the additional emission at 60 $\mu$m from the H II region. If this is the case, their true positions on the *IRAS* color-color diagram should be to the right of their apparent positions and close to the T Tauri box, as suggested in Paper I. Another explanation for their *IRAS* colors is that the type II sources are made up of multiple components in different evolutionary stages or with different masses and have colder components which are more luminous at 60/100 $\mu$m (e.g., class I sources of Lada 1987) and warmer components which are more luminous at shorter wavelengths (e.g., class II sources). If the warm sources have sufficiently large luminosities at 12 $\mu$m, it could produce the type II color indices. In fact, sources Nos. 5 and 44 of Paper I and No. 52 in the present paper, which, however, are not of type II, are reported to be multiple systems, one/some of the component(s) peaking at near-infrared in the spectral energy distributions (Ressler & Shure 1991; Skrutskie et al. 1992; Graham & Heyer 1989). For the type II sources, this situation could also be the case.

In Paper I, we mentioned that sources Nos. 7, 12, and 13 might be associated with molecular outflows based on the CO($J$ = 2–1) observations. The associations with molecular outflows of these sources and, further, of sources Nos. 19 and 34, have been confirmed by the CO($J$ = 3–2) observations with the KOSMA 3 m telescope, whose results are presented in Appendix. All of them are type II sources except for No. 34 which is of type III. These results also suggest that many of type II sources are stellar objects.

The type III sources are poorly detected at 60 $\mu$m and some of them also at 100 $\mu$m. Since their 12/25 $\mu$m color indices are not always warm like type II sources, they possibly have spectral energy distributions similar to those of the type I sources, but have unfavorable detection conditions at 60/100 $\mu$m due to the contamination by the extended emission from the H II region or to the multiplicity of the sources, like in the case of the type II sources. One type III source, No. 54, is associated with an HH object and a molecular outflow (HH 132; Ogura 1990; Iwata et al. 1994), although only an upper limit is given for its 60 $\mu$m flux.

### 4.3. *Star Formation in the Bright-rimmed Clouds*

The 19 *IRAS* sources selected here have a luminosity range of $\sim$20 to $3 \times 10^4\ L_\odot$ with an average of $\sim 10^3\ L_\odot$ (Fig. 4). The typical luminosities of the *IRAS* sources associated with Bok globules and dense cores of cloud complexes are $\sim 3\ L_\odot$ (Sugitani et al. 1989) and $\sim 1\ L_\odot$ (Beichman et al. 1986), respectively. This comparison suggests, in agreement with the result in Paper I, that either single stars of intermediate mass or multiple systems of low-mass stars are more preferentially formed in bright-rimmed clouds than in Bok globules and dense cores. At present it is not known which case is more general. Systematic imaging observations with an IR camera will answer this question in the near future. At the same time, however, it should be mentioned that since the detection limit of the *IRAS* point sources in our surveys is probably around $10\ L_\odot$ as suggested in Paper I, it is very likely that we have missed some low-mass stars embedded in bright-rimmed clouds. The type C clouds have sources of lower luminosities, $\sim 10\ L_\odot$ on the average, than the types A and B clouds, suggesting the formation of somewhat lower mass stars.

Again following Paper I, we have calculated *IRAS* luminosities *normalized* to unit cloud mass, $L_{\rm IR}/M'_{\rm cloud}$. The result shows that $L_{\rm IR}/M'_{\rm cloud}$ ranges between $\sim$0.01 and $10^2\ L_\odot/M_\odot$, as illustrated in Figure 5. The logarithmic average of the 19 clouds is 0.57 ($3.7\ L_\odot/M_\odot$), which is much larger than the typical values for isolated Bok globules, $\sim 0.1\ L_\odot/M_\odot$ (Sugitani et al. 1989), and the dense cores having similar masses, $\sim 0.03\ L_\odot/M_\odot$ ($\sim 1\ L_\odot$: Beichman et al. 1986; $\sim 30\ M_\odot$: Myers, Linke, & Benson 1983). This result is consistent with those of Paper I and of Sugitani et al. (1989), and implies a higher efficiency of star formation in the bright-rimmed cloud. The logarithmic averages for the rim types A, B, and C are $0.91 \pm 1.42$ (12), $0.15 \pm 0.45$ (5), and $-0.33 \pm 0.11$ (2),

© American Astronomical Society • Provided by the NASA Astrophysics Data System

1994ApJS...92..163S



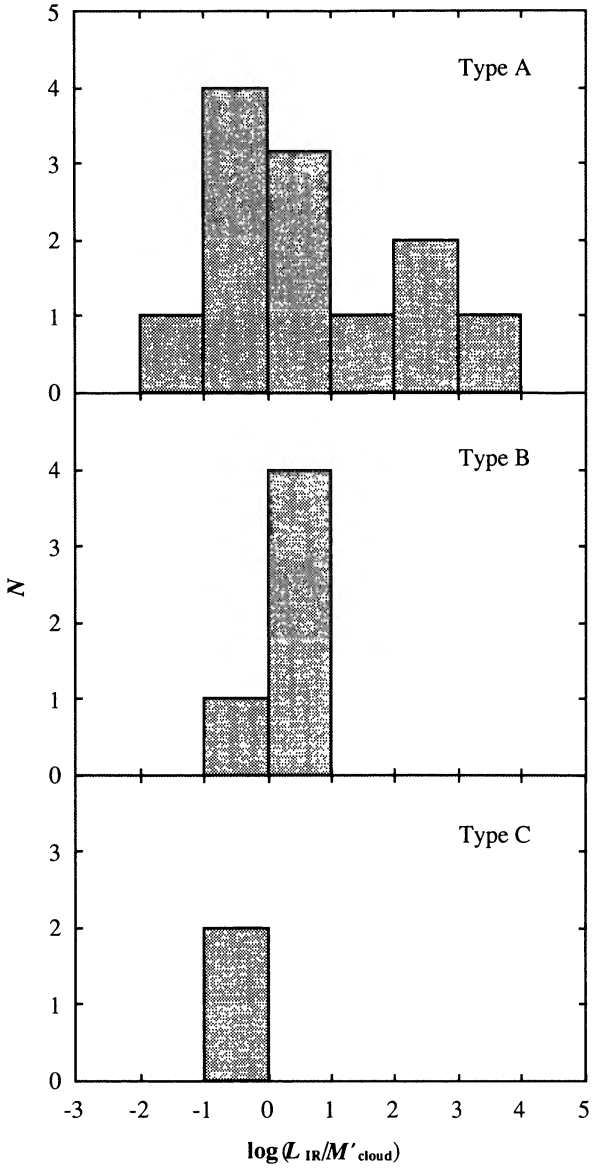


FIG. 5.—Distribution of *IRAS* luminosity to mass ratios. The masses are estimated from the cloud radii assuming a constant density (see text).

respectively. Although the differences are small, this suggests a tendency that flatter bright-rimmed clouds have higher star formation efficiency. Elmegreen (1993) pointed out that a converging shock could trigger star formation before a cloud attains a cometary shape, depending on the density distribution in the ionized gas and the molecular cloud. The rim shape presumably makes a difference in the build-up of the core and the subsequent mass accretion, resulting in the difference in the mass of the star formed (see above) as well as in the efficiency of star formation.

### 4.4. *Frequency of Star Formation by Radiation-driven Implosions*

The number of the bright-rimmed clouds with *IRAS* sources per H II region varies from 1 to 6 in this work. The average number per H II region is 2.0 for all the 45 clouds and 2.8 for the 25 clouds selected by the same criteria used in Paper I, where the average was 2.4. The number of the bright-rimmed clouds with $d \leq 2$ kpc is 21 out of the 25 clouds in this work, which is well compared to 41 in Paper I if we take into account the difference in the sky areas covered. Therefore, one of the main arguments of Paper I that a considerable number of stars are formed in the bright-rimmed clouds around H II regions through radiation-driven implosion is unchanged (see § 4.3 of Paper I for the details). This seems to be quite natural. If molecular clouds are composed of a number of clumps having various masses as suggested by many studies (e.g., Tatematsu et al. 1993) and if OB stars are formed there, star formation by radiation-driven implosion must be inevitable; the physical conditions of such clumps exposed to UV radiations from the OB stars well match those predicted by the models of the radiation-driven implosion (Klein, Sandford, & Whitaker 1985; Bertoldi 1989; Elmegreen 1993, and references therein).

## 5. SUMMARY

We have extended our survey for small bright-rimmed clouds associated with *IRAS* point sources (Sugitani et al. 1991) to the southern sky in order to improve the statistics obtained in the northern sky on star formation induced by radiation-driven implosion. The ESO(R)/SERC(J) Atlases and *IRAS* Point Source Catalog have been used. The main findings of this survey are as follows:

1. Forty-five bright-rimmed clouds associated with *IRAS* point sources have been selected from the 22 H II regions listed in Table 1.
2. Four of the 45 bright-rimmed clouds are associated with HH objects. Three clouds out of the four are associated with molecular outflows.
3. About 80% of the bright-rimmed clouds have small radii of $\lesssim$0.5 pc, which are similar to those of Bok globules or dense cores in dark cloud complexes. Forty percent of the clouds appear to have small masses of $\lesssim 100\ M_\odot$.
4. About 40% of the associated *IRAS* sources have spectral energy distributions of the type I (core samples). About 30% have spectral energy distributions of the type II, which resemble those of hot cirrus sources, but they are considered to be stellar objects on the basis of the high *IRAS* correlation coefficients and of the molecular/optical outflows associated with some of them.
5. The associated *IRAS* sources have luminosities of $\sim$20 to $3 \times 10^4\ L_\odot$, which are on the average about three orders of magnitude larger than those of the *IRAS* sources associated with Bok globules or dense cores and are one order of magnitude larger than the result obtained in Paper I. The latter difference may be caused in part by the inclusion of more distant sources in this work. The former implies that bright-rimmed clouds tend to form either single stars of higher mass or more multiple stars than Bok globules and dense cores.
6. The *IRAS* luminosity per unit cloud mass, $L_{\rm IR}/M_{\rm cloud}$, is also larger in the bright-rimmed clouds by about two orders of magnitude than in dark globules or dense cores. This indicates a higher efficiency of star formation in bright-rimmed clouds.
7. A significant number of bright-rimmed clouds are sites of

© American Astronomical Society • Provided by the NASA Astrophysics Data System

1994ApJS...92..163S



TABLE 5

BRIGHT-RIMMED CLOUDS ASSOCIATED WITH MOLECULAR OUTFLOWS

| Cloud Number | $\alpha$ (1950) | $\delta$ (1950) | *IRAS* Source | *IRAS* Type |
|---|---|---|---|---|
| 7 ..... | $2^h31^m01^s7$ | 61°33'40" | 02310+6133 | II |
| 12 ..... | 2 51 08.3 | 60 23 35 | 02511+6023 | II |
| 13 ..... | 2 57 03.6 | 60 28 29 | 02570+6028 | II |
| 19 ..... | 5 32 00.4 | −3 00 12 | 05320−0300 | II |
| 34 ..... | 21 32 02.5 | 57 50 06 | 21320+5750 | III |

star formation, and it is suggested that the process through which these stars form is radiation-driven implosion.

8. It is very important to definitely confirm the last statements through systematic surveys by IR imaging and extensive dynamical studies in the radio wavelengths for many bright-rimmed clouds.

We would like to thank Kiso Observatory for permitting us to use the dark room facilities and the computer. One of us (K.S.) would like to thank Prof. Gisbert Winnewisser for the machine time on the KOSMA 3 m radio telescope, and also other staff members and students of KOSMA for helpful supports. This work was financially supported in part by the Grant-in-Aid for Scientific Research by the Ministry of Education, Science, and Culture (04740132).

## APPENDIX

## A MOLECULAR OUTFLOW SURVEY OF THE BRIGHT-RIMMED CLOUDS IN THE NORTHERN SKY

A molecular outflow survey of the northern bright-rimmed clouds with *IRAS* point sources have been carried out with the KOSMA (Kölner Observatorium für Submillimeter Astronomie) 3 m telescope in order to look for evidence that they, particularly those with *IRAS* sources of type II/III, are really young stellar objects. First in 1990 October and December, we searched for outflows in CO($J$ = 2–1) in all the clouds, excluding those where outflows had been found previously. Signs of outflow were found for clouds Nos. 7, 12, 13, 19, and 34, for which we made mapping in CO($J$ = 3–2) in 1991 February and confirmed the outflow associations (Table 5). The beam widths of the KOSMA telescope are 2'.2 at 230 GHz and 1'.5 at 345 GHz, respectively. The details of the telescope, receivers and spectrometers are described in Winnewisser et al. (1986, 1990) and Schieder et al. (1989).

Their CO($J$ = 2–1, and/or $J$ = 3–2) outflow profiles are shown in Figure 6. The CO($J$ = 3–2) outflow maps for the clouds Nos. 12 and 19 are shown in Figure 7, together with their optical images reproduced from the POSS red prints. Except for cloud No. 34, they are all associated with type II sources, which have warm 12/25 $\mu$m colors similar to that of a hot cirrus. Cloud No. 34 is associated with a type III source, which is poorly detected at 60 and 100 $\mu$m. Including these sources, 19 (20%) of the altogether 89 bright-rimmed clouds that we cataloged in both the northern and southern sky have hitherto been known to be associated with molecular outflows and/or HH objects, both of which are good signposts of young stellar objects.

## REFERENCES

Ardeberg, A., & Maurice, E. 1980, A&AS, 39, 325
Beichman, C. A. 1983, in Light on Dark Matter, ed. F. P. Israel (Dordrecht: Reidel), 279
Beichman, C. A., Myers, P. C., Emerson, J. P., Harris, S., Mathieu, R. D., Benson, P. J., & Jennings, R. E. 1986, ApJ, 307, 337
Beichman, C. A., Neugebauer, G., Habing, H. J., Clegg, P. E., & Chester, P. E., eds. 1988, IRAS Catalogs and Atlases, Vol. 1, Explanatory Supplement (Washington, DC: US GPO)
Bertoldi, F. 1989, ApJ, 346, 735
Bertoldi, F., & McKee, C. F. 1990, ApJ, 354, 529
Cernicharo, J., Bachiller, R., Duver, G., González-Alfonso, E., & Gómez-González, J. 1992, A&A, 261, 589
Chernin, L. M., & Masson, C. R. 1991, ApJ, 382, L93
Chini, R. 1981, A&A, 99, 346
Elmegreen, B. G. 1993, in Proc. Canary Island Winter School of Astrophysics, Star Formation in Stellar Systems, ed. G. Tenorio-Tagle, M. Prieto, & F. Sánchez (Cambridge Univ. Press), 395
Georgelin, M., & Georgelin, Y. P. 1976, A&A, 49, 57
Georgelin, M., Georgelin, Y. P., & Roux, S. 1973, A&A, 25, 337
Graham, J. A. 1986, ApJ, 302, 352
Graham, J. A., & Heyer, M. H. 1989, PASP, 101 573
Herbst, W. 1975a, AJ, 80, 212
———. 1975b, AJ, 80, 503
Herbst, W., & Havlen, R. J. 1977, A&AS, 30, 279
Herbst, W., Miller, D. P., Warner, J. W., & Herzog, A. 1982, AJ, 87, 98
Iwata, T., et al. 1994, in preparation
Joint *IRAS* Science Working Group 1988, The Point Source Catalog, Version 2 (Washington, DC: US GPO)
Kilambi, G. C. 1977, MNRAS, 178, 423
Klein, R. I., Sandford, M. T., & Whitaker, R. W. 1985, in Protostars and Planets II, ed. D. C. Black & M. S. Matthews (Tucson: Univ. of Arizona Press), 340
Lada, C. 1987, in IAU Symp. 115, Star-forming Regions, ed. M. Peimbert & J. Jugaku (Dordrecht: Reidel), 1
Myers, P. C., Fuller, G. A., Mathieu, R. D., Beichman, C. A., Benson, P. J., Schild, R. E., & Emerson, J. P. 1987, ApJ, 319, 340
Myers, P. C., Linke, R. A., & Benson, P. J. 1983, ApJ, 264, 517
Nakano, M., Ogura, K., Sugitani, K., & Lijeström, T. 1994, in preparation
Ogura, K. 1990, PASP, 102, 1336
Ogura, K., & Walsh, J. R. 1991, AJ, 101, 185
Ogura, K., & Walsh, J. R. 1992, ApJ, 400, 248
Olberg, M., Reipurth, B., & Booth, R. S. 1992, A&A, 259, 252
Patel, N. A., Xie, T., & Goldsmith, P. F. 1994, ApJ, 413, 593
Petterson, B. 1984, A&A, 139, 135
Reipurth, B., & Heathcote, S. 1991, A&A, 246, 511
Ressler, M. E., & Shure, M. 1991, AJ, 102, 1398
Schieder, R., Tolls, V., & Winnewisser, G. 1989, Exp. Astron., 1, 101
Schwartz, R. D., 1977, ApJ, 212, L25
Seggewiß, W., 1968, Veröff Astron. Inst. Bonn, No. 79
Skrutskie, M. F., Meyer, M. R., Carrasco, L., Cruz-Conzalez, I., Salas, L., Johnson, P., & Spillar, E. 1991, BAAS, 23, 1374
Space Telescope Science Institute. 1989, Guide Star Catalog, Version 1
Sugitani, K., Fukui, Y., Mizuno, A., & Ohashi, N. 1989, ApJ, 342, L87
Sugitani, K., Fukui, Y., & Ogura, K. 1991, ApJS, 77, 59 (Paper I)
Tatematsu, K., et al. 1993, ApJ, 404, 643
Tauber, J. A., Lis, D. C., & Goldsmith, P. F. 1993, ApJ, 403, 202
Turner, D. G. 1985, ApJ, 292, 148
Winnewisser, G., et al. 1986, A&A, 167, 207
Winnewisser, G., Zimmermann, P., Hernichel, J., Shieder, R., & Ungerechts, H. 1990, A&A, 230, 248

© American Astronomical Society • Provided by the NASA Astrophysics Data System

1994ApJS...92..163S

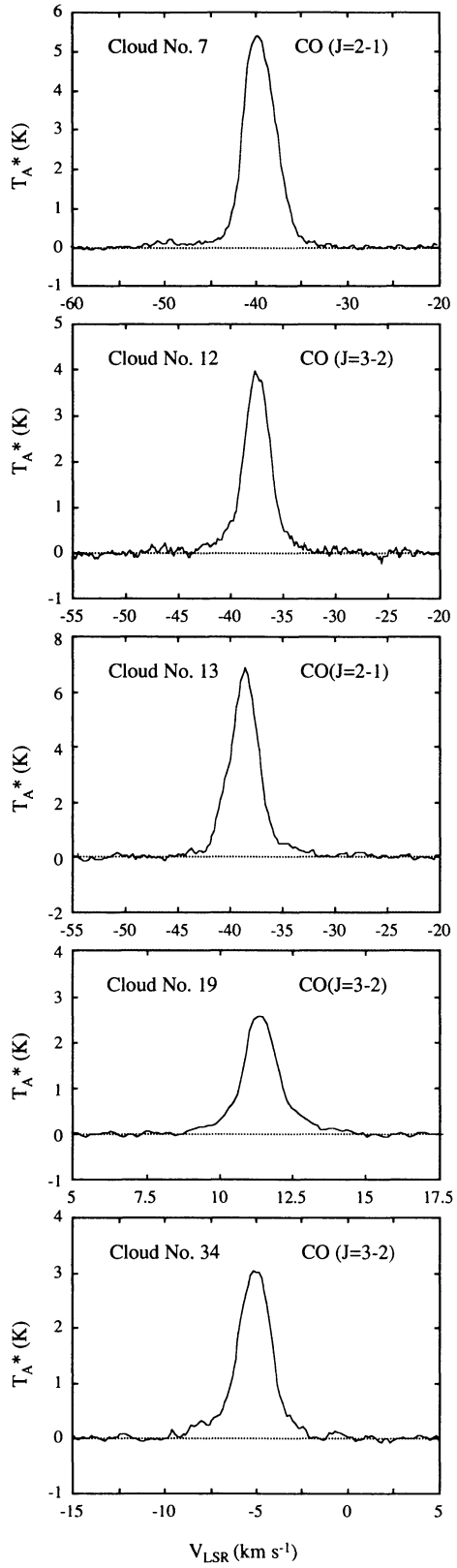


FIG. 6.—CO($J$ = 2–1 / $J$ = 3–2) profiles of the northern bright-rimmed clouds which were confirmed to be associated with molecular outflows.

© American Astronomical Society • Provided by the NASA Astrophysics Data System

1994ApJS...92..163S

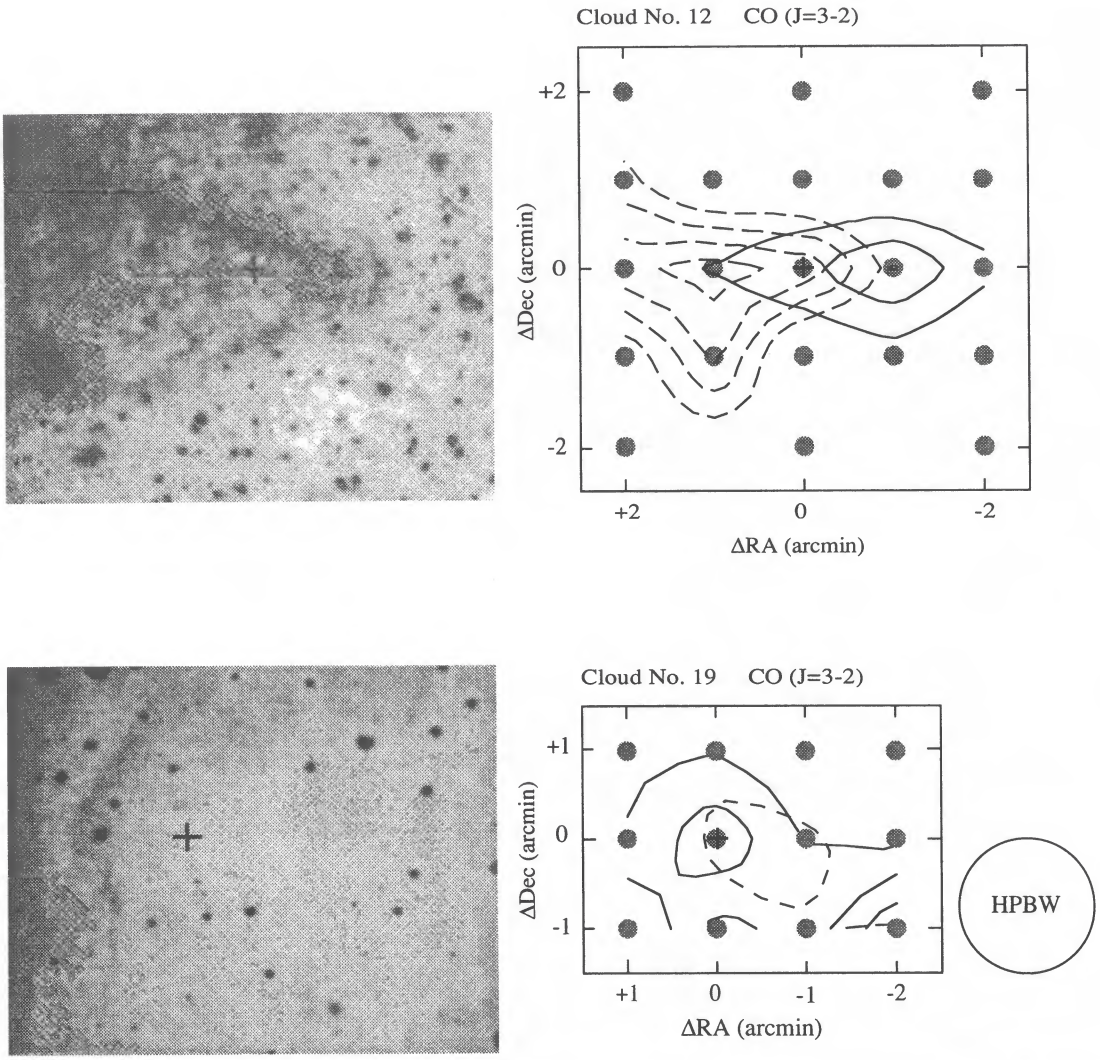


FIG. 7.—Two examples of the CO($J$ = 3–2) maps of the outflows. The attached optical images are reproduced from the POSS red prints with the same scale and orientation as the maps. Observed points are indicated by hatched dots and the *IRAS* positions by crosses. Blue lobes are shown by dashed contours and red ones by solid contours. The integrated velocity ranges are −46 to −40 km s$^{-1}$ (blue) and −34.5 to −28.5 km s$^{-1}$ (red) for cloud No. 12, and 7 to 10 km s$^{-1}$ (blue) and 12.5 to 15.5 km s$^{-1}$ (red) for cloud No. 19, respectively. The base levels and the contour intervals are 0.4 and 0.2 K km s$^{-1}$ for cloud No. 12, and 0.15 and 0.15 K km s$^{-1}$ for cloud No. 19, respectively.

© American Astronomical Society • Provided by the NASA Astrophysics Data System